EMITOR: Jurnal Teknik Elektro

Stator Design Analysis of Induction Motors to Improve Efficiency and Reduce Torque Ripple Using the Taguchi Method

Ferdyanto[1,*], Muhammad Raihan Fadhlurrahman[2], Wildan Hakim[3], R. Danuprawira Harris[4], Mario Roal[5]
[1,2,3,4]Department of Electrical Engineering – Universitas Pembangunan Nasional Veteran Jakarta
[5]Department of Electrical Engineering – Politeknik Negeri Pontianak
Jakarta, Indonesia
*ferdy@upnvj.ac.id

Abstract – *Three-phase induction motors dominate industrial applications due to their robustness, simple construction, and low maintenance requirements; however, torque ripple and efficiency degradation remain critical issues affecting vibration, acoustic noise, mechanical stress, and overall energy consumption. Excessive torque ripple may reduce operational stability and shorten motor lifespan, while low efficiency increases electricity costs in continuous industrial processes. Conventional optimization approaches often address torque ripple or efficiency separately and usually require extensive computational effort with a large number of simulation iterations. This study proposes an integrated optimization framework combining Finite Element Analysis (FEA) and the Taguchi method to simultaneously reduce torque ripple and improve efficiency through systematic stator design modification. Six control factors are evaluated, including slot geometry parameters (hs0, hs2, bs1, bs2), stator core material, and air-gap length, arranged using an L25 orthogonal array to minimize simulation runs while maintaining statistical reliability. Electromagnetic simulations are performed using ANSYS Maxwell to obtain torque characteristics, magnetic behavior, power loss, and efficiency under rated operating conditions. Statistical evaluation through Analysis of Means (ANOM) and Analysis of Variance (ANOVA) identifies dominant parameters and determines the optimal design combination. Results indicate that stator core material contributes most significantly, accounting for 77.89% of torque ripple variation and 69.24% of efficiency variation, followed by slot width parameters and air-gap length. The optimized design reduces torque ripple from 17.27% to 17.13% and increases efficiency from 86.58% to 88.52%, while reducing total power losses by 2.25 kW. In addition, the optimized design provides smoother torque response and more stable operation during startup and steady-state conditions. The proposed approach demonstrates a computationally efficient and statistically robust method for industrial induction motor design, offering practical applicability for improving energy efficiency, reliability, and operational stability.*

Keywords – *Finite Element Analysis (FEA); efficiency; stator design; Taguchi method; torque ripple.*

I. Introduction

THREE-phase induction motors are widely used in industrial systems because of their high reliability, simple construction, and low maintenance requirements [1]. It is estimated that more than 60% of industrial electricity consumption is associated with motor operation, making efficiency improvement essential for reducing operational costs and carbon emissions [2]. However, torque ripple, which refers to periodic variations in electromagnetic torque, can cause excessive vibration, acoustic noise, and mechanical wear, thereby reducing motor performance and shortening its operational lifespan [3]. In induction motors, the complex distribution of magnetic flux and the presence of harmonic currents make torque ripple mitigation more challenging than in permanent magnet machines [4].

Previous studies on induction motors have investigated digital modeling using Finite Element Analysis (FEA) to evaluate flux distribution and performance characteristics. Nevertheless, limited attention has been given to the simultaneous optimization of torque ripple and efficiency [1]. Torque ripple reduction strategies reported in the literature include direct torque control techniques, which have been shown to reduce ripple and improve the performance of induction motor drives [5]. Experimental studies have also demonstrated measurable ripple suppression and efficiency improvement through intelligent control strategies [6]. However, the comprehensive integration of statistical design of experiments, such as the Taguchi method, with FEA simulations for industrial three-phase induc-

The manuscript was received on May 23, 2026, revised on June 12, 2026, and published online on July 31, 2026. Emitor is a Journal of Electrical Engineering at Universitas Muhammadiyah Surakarta with ISSN (Print) 1411 – 8890 and ISSN (Online) 2541 – 4518, holding Sinta 3 accreditation. It is accessible at https://journals2.ums.ac.id/index.php/emitor/index.

tion motors remains relatively underexplored [7].

The Taguchi method provides an efficient Design of Experiments (DOE) framework by using orthogonal arrays to evaluate multiple control factors with significantly fewer experimental or simulation runs. This approach can reduce the number of required simulations by up to 75% compared with full factorial designs while maintaining acceptable accuracy of the results [8]. In electric motor applications, Taguchi-based DOE has been effectively used to optimize design parameters, reduce undesirable torque characteristics, and improve performance metrics in various motor types [9]. However, its application to torque ripple reduction and efficiency improvement in three-phase induction motors remains limited.

Finite Element Method (FEM) is a numerical technique capable of modeling the electromagnetic behavior of electrical machines with high accuracy. It can capture nonlinear material properties and complex boundary conditions required for accurate prediction of torque, losses, and efficiency [10]. Integrated FEA and optimization studies in electrical machine research have demonstrated significant improvements in motor performance. For example, induction motor analyses involving optimized rotor slot geometry and simulation-based design have shown substantial reductions in torque ripple and improved operational stability in electric drive applications [11–13].

This study aims to analyze the torque ripple and efficiency of a three-phase induction motor using an integrated Finite Element Analysis (FEA) and Taguchi optimization approach. Numerical simulations are conducted using electromagnetic FEA to model the motor under various geometric parameter configurations. Key design parameters related to stator and rotor geometry are systematically varied based on Taguchi orthogonal arrays to evaluate their influence on torque ripple and efficiency with a minimum number of simulation runs. Performance data, including electromagnetic torque, torque ripple percentage, power losses, and efficiency, are extracted from each simulation case for comparative analysis. The results of this study are expected to identify the optimal combination of design parameters that minimizes torque ripple while simultaneously improving energy efficiency, thereby contributing to enhanced performance, reliability, and operational stability of three-phase induction motors for industrial applications.

II. Research Methods

This research adopts a systematic computational methodology to analyze and optimize the stator design of a three-phase induction motor, with the primary objective of reducing electromagnetic torque ripple. The proposed approach integrates Finite Element Analysis (FEA) and the Taguchi optimization method to ensure both electromagnetic evaluation accuracy and design optimization efficiency. The overall research flow begins with the development of an initial motor model, which serves as the baseline for performance comparison, followed by a structured optimization and validation process.

First, the initial design of the three-phase induction motor is established based on standard industrial specifications and design guidelines. The motor geometry, including the stator, rotor, air gap, and winding configuration, is modeled using ANSYS Maxwell. Material properties, such as the nonlinear magnetic characteristics of the stator and rotor cores, are defined using B–H curves to accurately represent magnetic saturation effects. The motor model is then simulated under rated operating conditions to obtain the baseline electromagnetic performance, including torque waveform, average torque, and efficiency.

Next, stator parameters that significantly influence torque ripple are identified as control factors in the optimization process [14]. These parameters include stator geometric characteristics, such as slot opening width, slot height, tooth width, and slot wedge height, which directly affect air-gap flux harmonics and electromagnetic torque behavior [15]. In addition to geometric factors, the material properties of the stator core, particularly magnetic permeability and saturation characteristics, are also considered because of their influence on flux distribution and nonlinear magnetic effects [16]. Furthermore, the air-gap length is identified as a critical parameter because it governs the coupling between stator and rotor magnetic fields and plays a significant role in determining the magnitude of torque ripple [17]. These parameters are selected based on theoretical considerations, literature review, and preliminary simulations. Each control factor is assigned several design levels within practical manufacturing constraints to ensure the feasibility and reliability of the optimized design. The Taguchi method is subsequently applied to organize the simulation experiments using an appropriate orthogonal array, enabling the independent evaluation of each parameter with a reduced number of simulation runs.

For each experimental case defined in the orthogonal array, transient electromagnetic simulations are performed using FEA to obtain torque characteristics. Torque ripple is calculated from the electromagnetic torque waveform and used as the primary performance indicator. The simulation results are then evaluated using Analysis of Means (ANOM) and Analysis of Variance (ANOVA) to identify the most influential stator design parameters and determine the optimal combination of parameter levels.

Finally, the optimized stator design obtained from the Taguchi analysis is re-simulated and compared with the initial design to validate the effectiveness of the proposed methodology. The comparison focuses on torque ripple reduction while ensuring that average torque and efficiency are not adversely affected. This structured research flow ensures a repeatable and efficient optimization process, providing a reliable framework for stator design improvement in three-phase induction motors.

i. Three-Phase Induction Motor

A three-phase induction motor is an AC electrical machine that converts electrical energy into mechanical energy through electromagnetic induction between the rotating magnetic field of the stator and the induced currents in the rotor [18]. The asynchronous operation of the motor occurs because the rotor speed is slightly lower than the synchronous speed of the stator magnetic field, generating relative motion that produces electromagnetic torque.

When a balanced three-phase voltage is applied to the stator windings, a rotating magnetic field is produced in the air gap. This field induces electromotive force in the rotor conductors, generating rotor currents that interact with the stator magnetic field to produce electromagnetic torque. In practical motors, the generated torque is not perfectly constant and exhibits periodic fluctuations known as torque ripple. Torque ripple can be influenced by harmonic components, magnetic saturation, and stator or rotor geometry. In this study, torque ripple is quantified using the peak-to-peak torque variation relative to the average torque, as expressed in (1).

$$T_{\text{ripple}} = \frac{T_{\max} - T_{\min}}{T_{\text{avg}}} \times 100\% \tag{1}$$

In (1), $T_{\max}$, $T_{\min}$, and T_{avg} represent the maximum, minimum, and average torque values over one operating cycle, respectively. Torque ripple has been shown to depend on stator current harmonics, control methods, and machine design characteristics.

ii. Initial Motor Design

The initial three-phase induction motor model used in this study is shown in Figure 1. The model is reconstructed based on previously published research [18] and is used as a validated baseline design rather than a newly developed motor configuration. The geometric dimensions, material properties, and rated operating conditions are maintained to ensure realistic industrial performance characteristics.

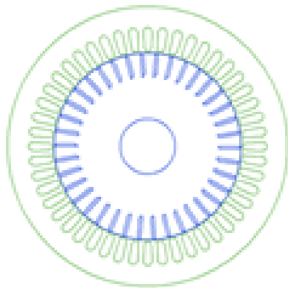

Figure 1: Initial three-phase induction motor design used as the baseline model.

As shown in Figure 1, the initial model functions as the reference configuration for comparative analysis. The primary contribution of this study lies in the systematic optimization of selected stator parameters using the Taguchi method integrated with Finite Element Analysis. The main parameters of the initial motor design are summarized in Table 1.

Table 1: Initial motor design parameters.

Parameter	Initial Design
Stator outer diameter [mm]	349
Stator inner diameter [mm]	235
Rotor outer diameter [mm]	233.6
Rotor inner diameter [mm]	70
Slot height, h_{s0} [mm]	0.7
Slot height, h_{s2} [mm]	22
Slot width, b_{s1} [mm]	10.5
Slot width, b_{s2} [mm]	12.5
Air-gap length [mm]	0.7
Rated speed [r/min]	1463
Core material	D23_50

Table 1 provides the baseline dimensions and operating specifications used for the initial simulation. These parameters are then used as the reference values for determining the range of design factor variations in the optimization process.

This study uses three main control-factor groups in the optimization process: stator slot geometry, stator core material, and air-gap length. Each factor is evaluated at predefined levels derived from the initial design and adjusted within practical manufacturing limits. Finite element simulations are conducted for all parameter combinations defined in the Taguchi design. The selected design variables and their respective levels are presented in Table 2.

As listed in Table 2, each design factor consists of five levels to support the Taguchi orthogonal array

Table 2: Design factor variables and levels.

Design Factor	Level 1	Level 2	Level 3	Level 4	Level 5
Slot height, h_{s0} [mm] [A]	0.3	0.4	0.6	0.7	0.8
Slot height, h_{s2} [mm] [B]	19	20	22	23	24
Slot width, b_{s1} [mm] [C]	8.5	9	9.5	10	10.5
Slot width, b_{s2} [mm] [D]	10.5	11	11.5	12	12.5
Core material [E]	Cobalt iron	Steel 1010	Steel 1018	M19_24G	Nickel iron
Air-gap length [mm] [F]	0.4	0.6	0.8	1.0	1.2

arrangement. After completing the simulations for all design-factor combinations, the resulting performance data are collected and evaluated. The influence of each design factor on the performance response is then examined through statistical analysis using the Analysis of Means approach.

iii. Data Analysis Using ANOM and ANOVA

After obtaining the simulation results for all experimental combinations defined by the Taguchi orthogonal array, the performance data are statistically analyzed to evaluate the influence of each design factor on torque ripple characteristics. Two statistical methods, namely Analysis of Means (ANOM) and Analysis of Variance (ANOVA), are employed to systematically interpret the simulation results and support the optimization decision-making process [19].

The Analysis of Means method is used to examine the effect of each design-factor level on the response variable. In this approach, the average torque ripple value is calculated for each level of every design factor. By comparing these mean values, the trend and sensitivity of torque ripple with respect to variations in stator slot geometry, core material properties, and air-gap length can be identified. The optimal level for each design factor is determined based on the level that produces the minimum mean torque ripple and the highest efficiency. The mean value of the response at each level is calculated using (2).

$$M = \frac{1}{n}\sum_{i=1}^{n} x_i \tag{2}$$

In (2), M denotes the mean value, n represents the total number of data points, i refers to the ith data point, and x_i corresponds to the output parameter data used in the analysis.

To further quantify the statistical significance of each design factor, ANOVA is applied to the simulation results. ANOVA decomposes the total variation of the response variable into the contribution of each design factor. Through this analysis, the percentage contribution of each factor to torque ripple variation can be calculated, allowing the dominant parameters influencing torque ripple to be identified [20]. Design factors with higher contribution percentages are considered more influential in the optimization process. The sum of squares for each factor is expressed in (3).

$$SSF_X = n\sum_{i=1}^{n}\left[m_{X_i}(Y) - m(Y)\right]^2 \tag{3}$$

In (3), SSF_X represents the sum of squares of factor X, Y denotes the output parameter, n is the total number of observations, $m_{X_i}(Y)$ is the mean response value of Y at the ith level of factor X, and $m(Y)$ is the overall mean response value. ANOVA is a statistical method used in experimental studies involving a continuous dependent variable and multiple experimental groups defined by one or more independent variables. Within ANOVA, the independent variables are referred to as factors, while the categories within each factor are known as levels. Furthermore, the robustness of the resulting optimized design is subsequently evaluated through validation simulation and comparison with the initial motor design.

III. Results and Discussion

The baseline design results present the electromagnetic performance of the initial three-phase induction motor before the optimization process is applied. These results serve as a reference for evaluating the effectiveness of stator design modifications in reducing torque ripple and improving efficiency. The baseline motor model is simulated under rated operating conditions using the Finite Element Method (FEM) to ensure an accurate representation of electromagnetic behavior.

Figure 2 shows the 2D finite element model of the three-phase induction motor developed in ANSYS Maxwell. The model includes detailed stator–rotor geometry, the air-gap region, and winding configuration under transient simulation conditions.

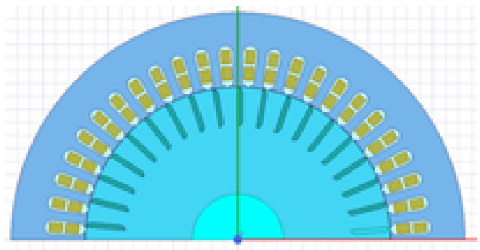

Figure 2: Two-dimensional sectional view of the three-phase induction motor model.

As shown in Figure 2, the finite element model provides a detailed representation of the electromagnetic structure required for performance evaluation. Unlike previous FEM studies, such as the work of Yetgin and Durmuş [18], which mainly focused on rotor slot variation, this study emphasizes stator geometry optimization combined with the Taguchi method. The refined air-gap mesh ensures accurate harmonic flux analysis, while the multi-parameter optimization approach enables simultaneous evaluation of geometry, material, and air-gap effects, providing more comprehensive and statistically robust results.

The baseline performance parameters obtained from the initial motor simulation are summarized in Table 3.

Table 3: Baseline motor performance.

Parameter	Value	Unit
Maximum torque	639.78	Newton meter (Nm)
Minimum torque	−290.49	Newton meter (Nm)
Torque ripple	17.27	%
Input power	96.23	kiloWatt (kW)
Output power	83.32	kiloWatt (kW)
Power loss	12.91	kiloWatt (kW)
Efficiency	86.58	%

Table 3 shows that the baseline motor produces an average torque of 538.69 Nm, with a maximum torque of 639.78 Nm and a minimum torque of −290.49 Nm. These values result in a torque ripple of 17.27%. The input power is 96.23 kW, while the output power is 83.32 kW, resulting in a total power loss of 12.91 kW and an efficiency of 86.58%. The torque response of the baseline motor is illustrated in Figure 3.

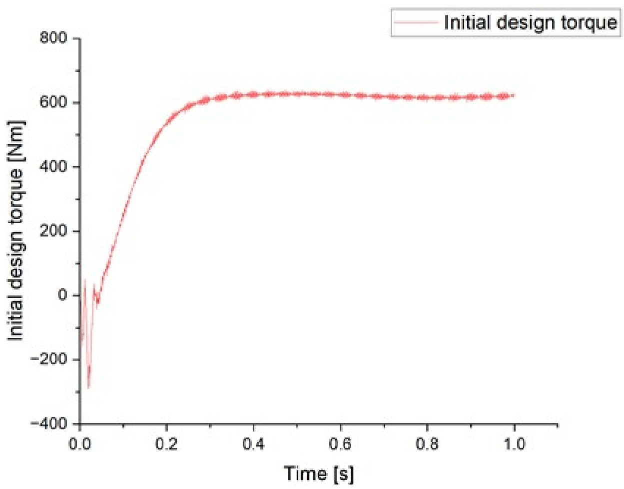

Figure 3: Torque response of the baseline motor design.

Figure 3 indicates that the baseline motor still experiences torque fluctuation during operation. This condition confirms the need for further stator design optimization to reduce torque ripple while maintaining acceptable efficiency and torque output.

After obtaining the torque ripple and efficiency results from the baseline design simulation, the study proceeds with the simulation of design factor variations using an L25 orthogonal array. The design factors considered in this research include Factor A, which represents the slot height h_{s0}; Factor B, the slot height h_{s2}; Factor C, the slot width b_{s1}; Factor D, the slot width b_{s2}; Factor E, the stator core material; and Factor F, the air-gap length.

All torque, current, voltage, and power waveforms are obtained directly from ANSYS Maxwell time-step simulation using the electromagnetic solver during motor operation from 0 to 1 s. The data are exported in time-series format and processed numerically to calculate peak torque, minimum torque, average torque, torque ripple percentage, and efficiency. An example of the torque response for simulation case 1 is shown in Figure 4.

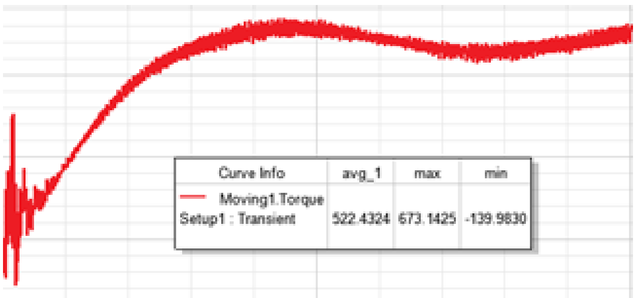

Figure 4: Torque response obtained from simulation case 1.

The torque response in Figure 4 provides the basis for extracting torque ripple characteristics from the transient electromagnetic simulation. In addition to torque response, power characteristics are also evaluated to determine the efficiency of each design configuration. The power response for simulation case 1 is presented in Figure 5.

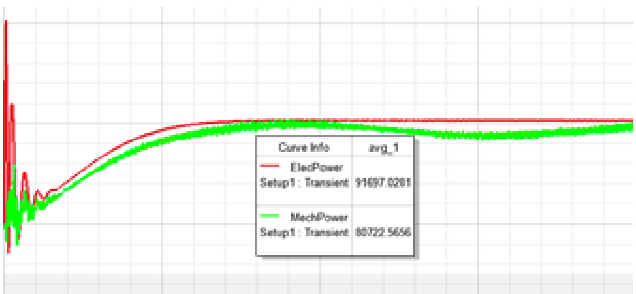

Figure 5: Power response obtained from simulation case 1.

Figure 5 shows the power behavior during the transient and steady-state operating regions. The extracted simulation results from all design combinations are summarized in Table 4.

Table 4 indicates that each design configuration arranged according to the Taguchi orthogonal array produces different torque ripple and efficiency values. These findings are subsequently used as the basis for determining the optimal parameters through ANOM and ANOVA. The ANOM result for torque ripple is

Table 4: Orthogonal array simulation results.

Simulation No.	Torque Ripple (%)	Efficiency (%)
1	15.564	88.03
2	18.995	86.73
3	18.420	84.86
4	17.483	77.06
5	17.045	88.47
6	19.004	85.31
7	15.427	89.69
8	15.815	88.44
9	18.532	82.33
10	18.369	83.33
11	18.760	85.02
12	18.741	85.93
13	18.753	80.53
14	14.234	89.67
15	16.090	87.90
16	15.732	89.30
17	16.537	88.03
18	17.569	84.22
19	18.103	83.93
20	17.583	79.82
21	18.815	85.75
22	18.336	85.47
23	16.316	88.96
24	17.338	87.15
25	18.186	80.36

shown in Figure 6.

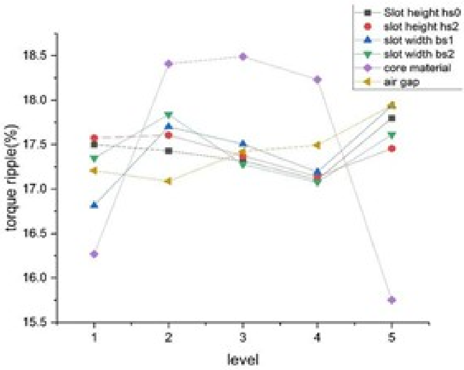

Figure 6: ANOM result of torque ripple for each design factor.

Figure 6 illustrates the effect of each design factor level on torque ripple. The optimal level for torque ripple is determined based on the level that produces the lowest mean response. To evaluate the influence of the design factors on efficiency, the corresponding ANOM result is presented in Figure 7.

As shown in Figure 7, the efficiency response varies with changes in stator geometry, core material, and air-gap length. After ANOM identifies potential optimal factor levels, ANOVA is applied to evaluate the significance and percentage contribution of each design factor. The SSF results for torque ripple and efficiency are listed in Table 5.

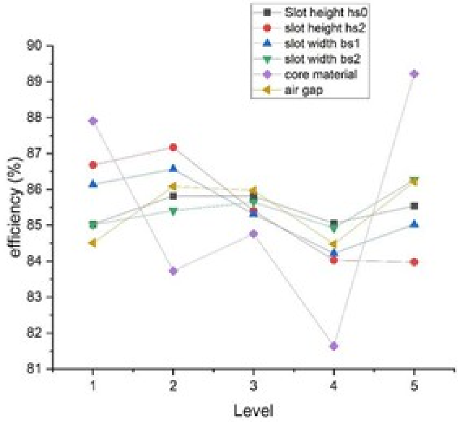

Figure 7: ANOM result of efficiency for each design factor.

Table 5: SSF results of torque ripple and efficiency.

Design Factor	Torque Ripple		Efficiency	
	SSF	Effect	SSF	Effect
A	1.296259	2.93%	3.028659	1.10%
B	0.706341	1.60%	43.365530	15.71%
C	3.857809	8.72%	17.212450	6.24%
D	1.770807	4.00%	5.851817	2.12%
E	34.455555	77.89%	191.100700	69.24%
F	2.151912	4.86%	15.439680	5.59%
Total	44.238680	100.00%	275.998800	100.00%

Table 5 shows that the stator core material has the most dominant influence on both torque ripple and efficiency. To provide a clearer interpretation of the ANOVA results, the percentage contribution of each design factor to torque ripple is illustrated in Figure 8.

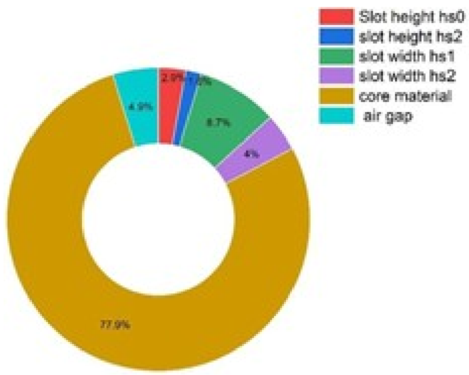

Figure 8: ANOVA percentage contribution of each design factor to torque ripple.

Figure 8 confirms that Factor E, namely the stator core material, contributes the highest percentage to torque ripple variation. The percentage contribution of each factor to efficiency is shown in Figure 9.

Based on Figure 9, the stator core material also provides the largest contribution to efficiency variation.

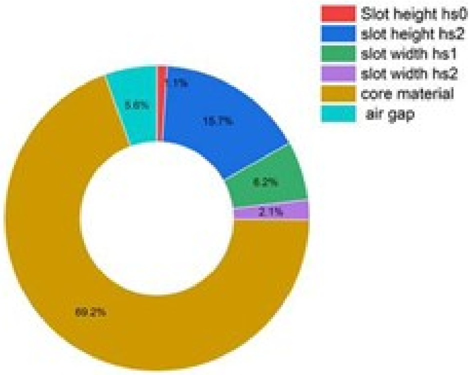

Figure 9: ANOVA percentage contribution of each design factor to efficiency.

The ANOM and ANOVA results show that h_{s0} and h_{s2} have moderate effects, with optimal levels at A4, corresponding to 0.7 mm, and B3, corresponding to 22 mm. Higher levels of b_{s1} and b_{s2}, namely C5 and D5, improve torque and efficiency while maintaining acceptable torque ripple. The stator core material is the most dominant factor, with nickel–iron at E5 providing the best overall performance. The air-gap length also has a significant influence, with F5, corresponding to 1.2 mm, yielding improved results. Therefore, the optimal combination is A4–B3–C5–D5–E5–F5.

Based on the optimization results, the optimized design is then re-simulated to evaluate its electrical and electromagnetic responses. The power response of the optimized design is shown in Figure 10.

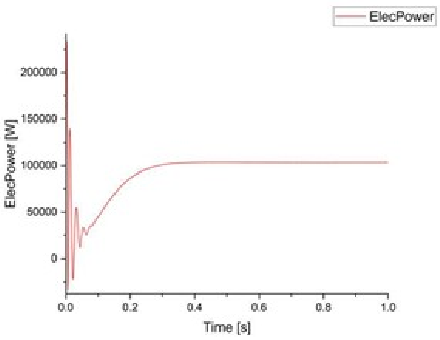

Figure 10: Power response chart of the optimized motor design.

Figure 10 indicates that the motor undergoes a highly dynamic transient phase at the beginning of operation, from 0 to 0.4 s. This phase is marked by an initial power spike that exceeds 200,000 W due to inrush current, followed by rapid decay of oscillations. After 0.4 s, the motor reaches a consistent steady-state condition, with power stabilizing in the range of approximately 103,000 to 104,000 W. The voltage response of the optimized motor design is presented in Figure 11.

Figure 11 shows that the electrical system of the

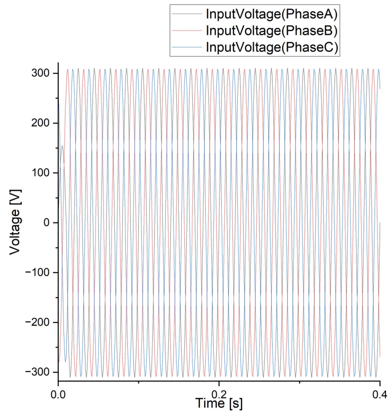

Figure 11: Voltage response chart of the optimized motor design.

motor demonstrates stable behavior, with the three-phase input voltages, namely Phase A, Phase B, and Phase C, maintaining a voltage amplitude of approximately 311 V peak-to-neutral during the entire one-second simulation period. The current response of the optimized design is shown in Figure 12.

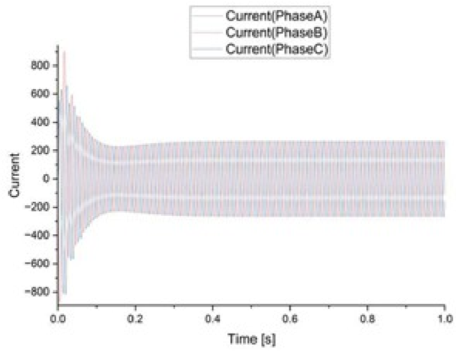

Figure 12: Current response chart of the optimized motor design.

As presented in Figure 12, the simulation results indicate stable motor operation under a constant three-phase input voltage of approximately 311 V. During startup, from 0 to 0.4 s, a high inrush current of approximately 900 A occurs, causing a temporary power surge above 200 kW to overcome load inertia. After this transient period, the oscillations rapidly decay, and the system reaches steady state at approximately 0.4 s with a stable current of approximately 250 A.

A comparative analysis of the output performance parameters between the initial motor design and the optimized motor design is presented in Table 6.

Table 6 demonstrates that the optimized design improves efficiency from 86.58% to 88.52%, indicating a more effective conversion of input power into mechanical output after optimization. At the same time, torque ripple decreases from 17.27% to approximately 17.13%, reflecting a smoother torque profile and im-

Table 6: Performance comparison between the optimized design and the initial design.

Parameter	Final Design	Initial Design	Change
Torque [Nm]	532.01	538.68	−6.67
Maximum torque [Nm]	626.20	639.78	−13.58
Minimum torque [Nm]	−285.00	−290.49	5.49
Torque ripple [%]	17.12	17.26	−0.1417
Input power [kW]	92.93	96.23	−3.30
Output power [kW]	82.26	83.32	−1.06
Power loss [kW]	10.66	12.91	−2.25
Efficiency [%]	88.52	86.58	1.94

proved operational stability of the induction motor. The torque comparison between the initial and optimized designs is illustrated in Figure 13.

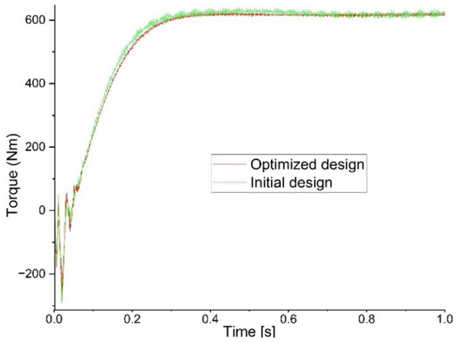

Figure 13: Torque comparison between the optimized design and the initial design.

Figure 13 shows the electromagnetic torque response of the induction motor for both the initial and optimized stator designs under rated conditions, obtained from transient FEA simulations in ANSYS Maxwell. During startup, from 0 to 0.2 s, both designs exhibit high torque oscillations. However, the optimized design demonstrates lower fluctuation amplitude, indicating improved harmonic suppression. In steady-state operation, after approximately 0.3 s, the optimized torque waveform becomes smoother with reduced peak-to-peak variation while maintaining nearly the same average torque. This confirms that the optimized design effectively reduces torque ripple without significantly degrading torque performance.

The magnetic flux distribution of the optimized three-phase induction motor design is analyzed to evaluate the effect of the optimization process on flux uniformity, torque ripple reduction, and overall motor performance. The flux vector distribution of the optimized design is shown in Figure 14.

Figure 14 shows that the optimized design exhibits a more uniform and symmetrical magnetic flux distribution across the stator teeth and air-gap region. To further evaluate the improvement achieved through optimization, the magnetic flux distribution of the initial design is presented in Figure 15.

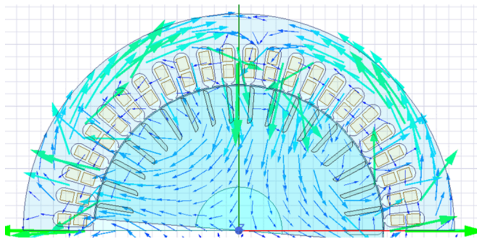

Figure 14: Flux vector distribution of the optimized motor design.

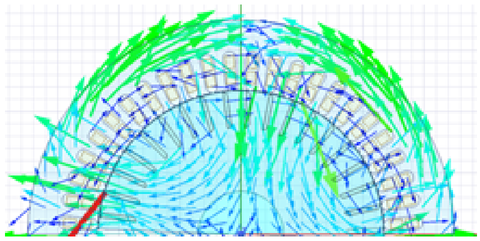

Figure 15: Flux vector distribution of the initial motor design.

Table 7: Optimized design parameters.

Parameter	Initial Design	Final Design
Stator outer diameter [mm]	349	349
Stator inner diameter [mm]	235	235.5
Rotor outer diameter [mm]	233.6	233.1
Rotor inner diameter [mm]	70	70
Slot height, h_{s0} [mm]	0.7	0.7
Slot height, h_{s2} [mm]	22	22
Slot width, b_{s1} [mm]	10.5	10.5
Slot width, b_{s2} [mm]	12.5	12.5
Air-gap length [mm]	0.7	1.2
Core material	D23_50	Nickel iron

A comparison between Figure 14 and Figure 15 indicates a clear improvement in magnetic flux distribution after optimization. In the initial design, non-uniform flux distribution can be observed in several regions of the stator teeth and air gap, as indicated by high flux density concentration and irregular flux vector directions. This condition suggests the presence of localized magnetic saturation and increased flux leakage, which contribute to fluctuations in electromagnetic forces and result in higher torque ripple.

In contrast, the optimized final design exhibits a more uniform and symmetrical magnetic flux distribution across the stator teeth and air gap. The improved homogeneity of flux density indicates that the geometric and material modifications effectively reduce excessive flux concentration and mitigate magnetic saturation. This enhanced flux distribution leads to a more stable electromagnetic force, thereby contributing to torque ripple reduction and overall motor performance improvement. The optimized motor design parameters are summarized in Table 7.

As shown in Table 7, the final optimized design maintains several baseline geometric parameters while modifying the air-gap length and core material. These modifications contribute to improved flux distribution, lower power loss, and higher efficiency while maintaining acceptable torque performance.

IV. Conclusion

This study successfully demonstrates that the integration of Finite Element Analysis and the Taguchi optimization method provides an effective and computationally efficient framework for improving the performance of a three-phase induction motor. The main problem addressed in this study is torque ripple and efficiency degradation caused by variations in stator geometric and material parameters. Statistical analysis confirms that the stator core material is the most dominant factor influencing both torque ripple and efficiency.

The optimized design increases efficiency from 86.58% to 88.52% and reduces torque ripple from 17.27% to 17.13%, while decreasing power losses by 2.25 kW. The main advantage of the proposed method is its ability to identify dominant design parameters using a reduced number of simulations through orthogonal array experimentation. However, the limitation of this study lies in the absence of experimental hardware validation and the relatively small percentage of torque ripple reduction. Future research should include prototype testing and multi-objective optimization considering thermal and mechanical constraints to further enhance industrial applicability.

Acknowledgment

The authors would like to express their sincere gratitude to the Electrical Energy Laboratory for providing facilities, software support, and technical assistance during the simulation and analysis process of this research. The support and guidance from the laboratory personnel greatly contributed to the successful completion of this study.

References

[1] P. Bozek, T. Krenicky, and V. Prajova, "Digital induction motor model based on the finite element method," *Applied Sciences*, vol. 13, no. 8, p. 5124, Apr. 2023. https://doi.org/10.3390/app13085124

[2] O. Ishnazarov, "Comprehensive energy saving strategies in industrial: Technical potentials for developing countries," vol. 3, no. 5, pp. 2155–2162, 2016.

[3] H. Feng, S. Zhang, J. Wei, X. Xu, C. Gao, and L. Ai, "Torque ripple reduction of brushless dc motor with convex arc-type permanent magnets based on robust optimization design," *IET Electric Power Applications*, vol. 16, no. 5, pp. 565–574, May 2022. https://doi.org/10.1049/elp2.12176

[4] J. A. Domínguez, N. Duro, and E. Gaudioso, "Finite element analysis of different transverse flux linear induction motor models to improve the performance of the main magnetic circuit," *Machines*, vol. 12, no. 2, p. 89, Jan. 2024. https://doi.org/10.3390/machines12020089

[5] Y. Zahraoui, "Induction motor dtc performance improvement by reducing flux and torque ripples in low speed," vol. 3, no. 1, pp. 93–100, 2022. https://doi.org/10.18196/jrc.v3i1.12550

[6] A. M. Prasetia, "Pengaturan kecepatan motor induksi tiga fasa dengan direct torque control menggunakan jaringan saraf tiruan," vol. 20, no. 2, pp. 24–32, 2022. https://doi.org/10.33795/eltek.v20i2.336

[7] C.-H. Lin, "Altered grey wolf optimization and taguchi method with fea for six-phase copper squirrel cage rotor induction motor design," *Energies*, vol. 13, no. 9, p. 2282, May 2020. https://doi.org/10.3390/en13092282

[8] L. Zhang, "Optimization of asynchronous motor with taguchi method based on finite element analysis," in *MATEC Web of Conferences*, vol. 382, Jun. 2023, p. 01010. https://doi.org/10.1051/matecconf/202338201010

[9] A. Farha, A. Zuchriadi, and M. A. Razi, "Mitor: Jurnal teknik elektro," *MITOR: Jurnal Teknik Elektro*, 2024.

[10] E. Schmidt, "Finite element analysis of electrical machines and transformers: State of the art and future trends," vol. 30, no. 6, pp. 1899–1913, 2011. https://doi.org/10.1108/03321641111168183

[11] M. Ozsoy, O. Kaplan, and M. Akar, "Fem-based analysis of rotor cage material and slot geometry on double air gap axial flux induction motors," vol. 15, no. November 2022, 2024. https://doi.org/10.1016/j.asej.2023.102393

[12] A. J. Ali, A. K. Shanshal, H. E. Aziz, and E. Hussain, "Characteristic optimization of three-phase induction motors based on fem," vol. 17, pp. 267–272, 2024.

[13] C. Ocak, "A fem-based comparative study of the effect of rotor bar designs on the performance of squirrel cage induction motors," 2023.

[14] J. Otypka, J. Sobra, and R. Pechanek, "The summary of induction motor torque ripple theories for motor torque analysis," no. 3.

[15] J. K. Kammoun, N. Ben Hadj, M. Ghariani, and R. Neji, "Torque ripple and harmonic density current study in induction motor: Two rotor slot shapes," vol. 8, no. April, pp. 197–204, 2015.

[16] A. F. Challoop, A. J. Sultan, and M. F. Bonneya, "Performance analysis of induction motor based on core material," 2021.

[17] I. K. Onwuka, P. I. Obi, O. Oputa, and C. S. Ezeonye, "Performance analysis of induction motor with variable air-gaps using finite element method," *NIPES Journal of Science and Technology Research*, vol. 5, no. 1, pp. 112–124, 2023. https://doi.org/10.5281/zenodo.7729203

[18] K. Thomas, A. Rahman, W. Rohouma, M. F. Ahamed, F. B. Shafi, M. Nahiduzzaman, and A. Khandakar, "Comprehensive fault diagnosis of three-phase induction motors using synchronized multi-sensor data collection," *Scientific Data*, vol. 12, p. 1468, 2025. https://doi.org/10.1038/s41597-025-05437-3

[19] F. Ferdyanto, G. Fatwa, A. Erlangga, and I. Marbawi, "Performance analysis of permanent magnet bldc motor for reducing cogging torque using taguchi method," *Elkha*, vol. 16, no. 1, p. 28, 2024. https://doi.org/10.26418/elkha.v16i1.76582

[20] M. W. Hisam, "The versatility of the taguchi method: Optimizing experiments across diverse disciplines," 2024.